

Electrodeposited Nickel Nanodots Array on the Silicon Wafer

Jin-Seung Jung,^{*} Eun-Mee Kim,[†] Weon-Sik Chae,[†] Leszek M. Malkinski,[‡]
Jin-Hee Lim,[‡] Charles O'Connor,[‡] and Jong-Ho Jun[§]

*Department of Chemistry, Kangnung National University, Gangneung 210-702, Korea. *E-mail: jjscm@kangnung.ac.kr*

[†]Korea Basic Science Institute, Gangneung Branch, Gangneung 210-702, Korea

[‡]Advanced Materials Research Institute, University of New Orleans, New Orleans, LA 70148, USA

[§]Department of Applied Chemistry, Kunkuk University, Chungju 380-701, Korea

Received August 11, 2008

Nanoporous anodic aluminum oxide (AAO) membrane has many advantages as a host material for a variety of magnetic materials. The magnetic materials can be embedded into the host pores by electrodeposition, sputtering, and infiltration routes. This work shows that the entire fabrication process to the magnetic nanomaterial through the AAO templating method can be thoroughly integrated with silicon technology. Thin aluminum film is directly deposited on the titanium precoated silicon wafer by dc sputtering. Subsequent two-step anodization of the aluminum film results in uniform morphology of the long-range ordered array of cylindrical alumina nanopores, which is used as a template for the electrochemical growth of the Ni nanodots array. The observed magnetic hysteresis loops at 10 K and room temperature show unique ferromagnetic coupling for the Ni nanodot array depending on field directions.

Key Words : Nickel nanodot, Electrodeposition, AAO membrane

Introduction

Various templates have attracted great interest in the preparation of a broad span of nanomaterials with desired morphologies.¹⁻⁷ Anodic aluminum oxide (AAO) is one of several types of membrane materials. The AAO membrane consists of a self-assembled hexagonal array of uniformly sized parallel cylindrical channels with the diameter ranging from several to hundreds of nanometers. The thickness of the AAO membrane, and thus the length of the cylindrical nanopores, can be varied from tens of nanometers to tens of micrometers. Recent studies report on the nanopatterning of magnetic materials by filling the nanopores of AAO template.^{8,9} Membranes filled with Co, Ni, and Fe have strong magnetic anisotropies, which are suitable for high density data storage materials.¹⁰⁻¹²

As a host material, thick AAO membrane has a good thermal, chemical, and mechanical stability, but thin AAO film is extremely brittle and difficult to handle. This problem can be solved by producing the porous membranes on a thick and solid substrate which does not deform easily and thus prevents crack formation. The aim of this work is to demonstrate that thin AAO film can be grown on a silicon substrate and magnetic nanomaterial can be embedded into its pores to fabricate hexagonal array of magnetic nanomaterial. Importantly, this provides opportunity to integrate the fabrication processes of thin AAO film and subsequent formation of magnetic nanodot with silicon technology, which ultimately enables to build more complex magnetic nanostructures on silicon wafers. In this work, we describe the microstructure of the thin AAO film and the magnetic properties of the deposited Ni nanodots array on a silicon wafer.

Experimental Section

Unlike the conventional method typically using thick aluminum foils, in this study, ultrathin AAO template film was fabricated by anodizing aluminum film deposited on a *n*-type Si wafer. Between the aluminum film and the Si wafer, thin Ti adhesion layer was introduced instead of Nb, which was used in the previous studies,^{13,14} as a conducting electrode for electrodeposition of Ni nanomaterial. The thickness of the Al film and the Ti buffer layer was about 1,000 and 100 nm, respectively (Fig. 1a). The Al/Ti bilayer was deposited by dc sputtering on a Si substrate. The pressure during deposition was maintained under 6×10^{-6} Torr. The sputtering power was 200 W and the deposition rate was about 1.5 nm/s. The anodizing was processed in a 0.3 M oxalic acid for 5 min at 5 °C under the constant voltage of 40 V. Since it is very difficult to make hexagonally well ordered AAO membrane in a single anodization process, multiple-step anodization processes were applied by repeating the anodization and the etching processes. Each etching process for the removal of generated thin aluminum oxide film was done in the aqueous mixture of phosphoric acid (5 wt%) and chromic acid (1.8 wt%) at 70 °C for 10 min. Magnetic material of Ni was electrodeposited at the bottom of the cylindrical nanopores of the AAO film on Ti-coated Si cathode against Pt anode under the constant current of 4 mA for 4 min at 20 °C, which was done in the aqueous electrolyte containing 8.4×10^{-2} M nickel chloride hexahydrate, 1.6 M nickel sulfamate tetrahydrate, and 0.3 M boric acid.

Microstructural analysis was carried out using a Hitach S-4700 field emission scanning electron microscope (FESEM). Magnetic property measurements were carried out with a

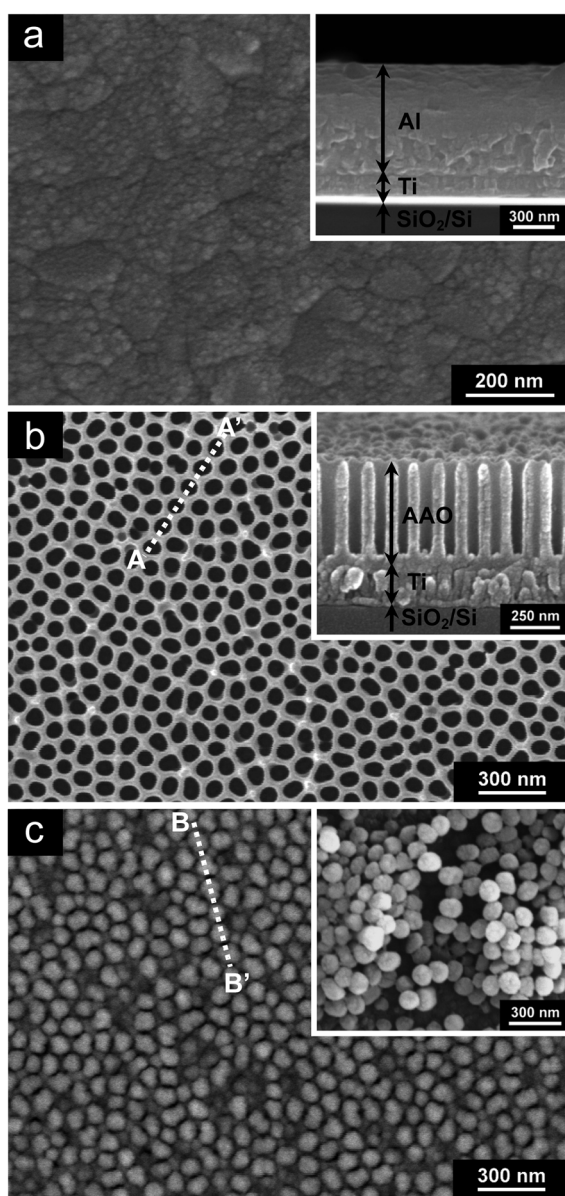


Figure 1. Top surface and cross-sectional (inset) images of (a) deposited Al and Ti layers on the Si wafer and (b) thin AAO template film on the Ti-coated Si wafer after pore widening. (c) Ni nanodots array on the Ti-coated Si wafer. Inset is a typical image for collected Ni nanodots.

superconducting quantum interference device magnetometer (SQUID; Quantum Design MPMS-5S). The hysteresis loops were measured at room temperature and 10 K in two different field configurations: the field in the wafer plane and the field normal to it.

Results and Discussion

Figure 1 shows the SEM images of the samples on the *n*-type Si wafer in different stages of the fabrication process. Figure 1a is typical morphologies of top surface and cross-section (inset) of the deposited Al film on the Ti-coated Si wafer. After subsequent multiple cycles of anodization-etching process, we could obtain a good quality of nano-

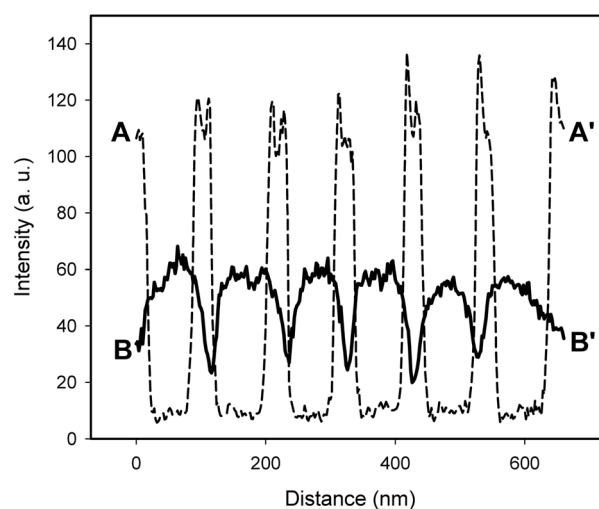


Figure 2. Intensity profiles of the AAO template film (dashed line) and the Ni nanodots array on the Ti-coated Si wafer (solid line), which are corresponding to the dotted lines as indicated in Figure 1b and 1c, respectively.

porous membrane with the vertical alignment of cylindrical nanopores on the Ti-coated Si wafer (Fig. 1b and inset). The average pore diameter, interpore spacing, and channel length (*i.e.* film thickness) of the fabricated AAO film are shown to be 80, 110, and 480 nm, respectively. Figure 1c shows Ni nanodot array on the Ti-coated Si wafer. Most of nickel nanodots are formed at the right position through the templating route, which is clearly supported by the image analysis (Fig. 2), even though a few defective voids are shown due to incomplete electrode contact at the bottom of alumina nanopores during electrodeposition. The resulting Ni nanodots with the average diameter and the interparticle spacing of 81 and 108 nm are well correlated to the average pore diameter (80 nm) and the interpore spacing (110 nm) of the AAO template film, respectively.

Figure 3 shows typical ferromagnetic hysteresis loops for the nickel nanodots. The coercive force and the saturation magnetization is almost same regardless of different field directions. This means that the electrodeposited Ni nano-material have no shape anisotropy, *i.e.* spherical shape, which is well agree to the spherical particle image shown in the inset of Figure 1c. The observed coercivity (H_c) of 160 Oe (at 10 K) is very similar with those of Ni nanostructures in the previous reports,¹⁵⁻¹⁷ which is decreased to 90 Oe with temperature increase to room temperature. One interesting point is that the initial slope of the hysteresis loop is more steep (*i.e.* higher squareness) in the case of field applied parallel to the membrane plane (\parallel) than that in the field normal to the plane (\perp). The squareness (S), which is the ratio between the remanent and the saturation moments, is shown to be $S_{\parallel} = 0.14$ and $S_{\perp} = 0.08$ at 10 K ($S_{\parallel} = 0.08$ and $S_{\perp} = 0.04$ at 300 K). If we imagine non-interacting spherical nanoparticles, it can be considered that the squareness should be same regardless of applied field directions. However, the observed different squareness implies that the Ni nanodot array can not be treated as ideal non-interacting

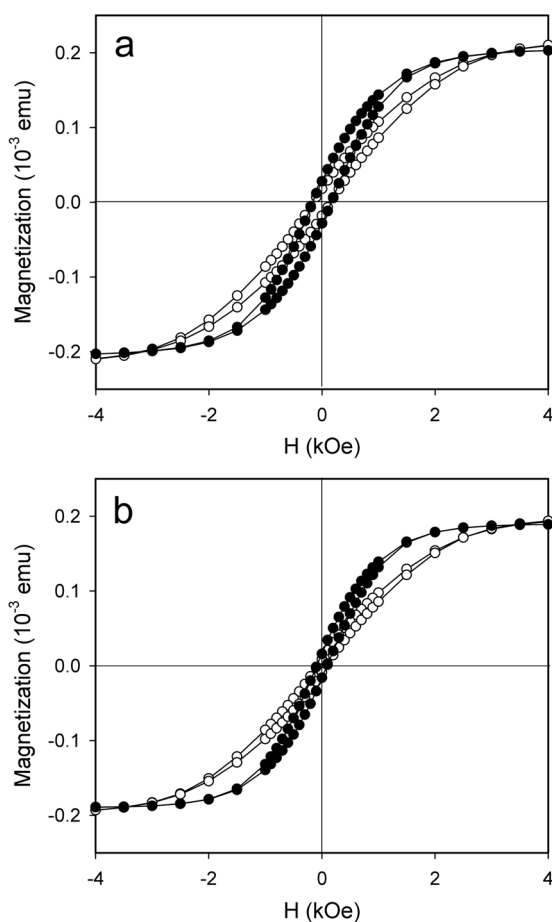


Figure 3. Hysteresis loops for Ni nanodots in the alumina template on Si wafer with the field applied parallel (●) and perpendicular (○) to the membrane plane at 10 K (a) and 300 K (b).

magnetic particles.

Theoretical model developed by Masuda *et al.*¹⁸ predicts that, in the case of high density planar array of magnetic nanoparticles, in-plane anisotropy overwhelm out-of-plane anisotropy as a result of strengthened magnetostatic couplings among dense in-planar nanoparticles. In this study, the particle density of the Ni nanodot array is $\sim 1 \times 10^{10}/\text{cm}^2$ with the interparticle spacing of 13.5 nm so that the magnetic coupling among the adjacent Ni nanodots can not be negligible. Hence, the observed higher squareness with the in-plane field means that there are interparticle magnetostatic couplings among the aligned Ni nanodots in the planar array. It is distinctly different from those of an isolated single dot or randomly oriented dot aggregate, and it could be controlled with the careful designs of interparticle distance and pattern structure.

In summary, magnetic Ni nanodots array was electrochemically grown on the Si wafer through AAO templating route. The advantage of this fabrication method for the Ni nanodot array is that it can be integrated with silicon technology. The observed magnetic data imply that there are in-planar magnetic couplings among the aligned Ni nanodots. A variety of magnetic materials, such as pure metals, metal alloys, and multilayered composites, can be considered as candidates for high density magnetic nanoparticle arrays.

Acknowledgments. This research was supported by the MKE (Ministry of Knowledge Economy), Korea, under the 2008 ITRC support program supervised by the IITA (IITA-2008-C1090-0801-0044) and the KBSI grant (N28083) to WSC.

References

1. Brumlik, C. J.; Menon, V. P.; Martin, C. R. *J. Mater. Res.* **1994**, *9*, 1174.
2. Martin, C. R. *Chem. Mater.* **1996**, *8*, 1739.
3. Marnakos, S. M.; Brousseau, L. C.; Jones, A.; Feldheim, D. L. *Chem. Mater.* **1998**, *10*, 1214.
4. Nishizawa, M.; Mukai, K.; Kuwabata, S.; Martin, C. R.; Yoneyama, H. *J. Electrochem. Soc.* **1997**, *144*, 1923.
5. Kyotani, T.; Tsai, L.-F.; Tomita, A. *Chem. Mater.* **1996**, *8*, 2109.
6. Raman, N. K.; Andreson, M. T.; Brinker, C. J. *Chem. Mater.* **1996**, *8*, 1682.
7. Wong, E. W.; Maynor, B. W.; Burns, L. D.; Lieber, C. M. *Chem. Mater.* **1996**, *8*, 204.
8. Jung, J.-S.; Lim, J.-H.; Choi, K.-H.; Oh, S.-L.; Kim, Y.-R.; Lee, S.-H.; Smith, D. A.; Stokes, K. L.; Malkinski, L.; O'Connor, C. J. *J. Appl. Phys.* **2005**, *97*, 10F306.
9. Jung, J.-S.; Jung, Y.-K.; Kim, E.-M.; Min, S.-H.; Jun, J.-H.; Malkinski, L. M.; Barnakov, Y.; Spinu, L.; Stokes, K. *IEEE Trans. Magn.* **2005**, *41*, 3403.
10. Whitney, T. M.; Jiang, J. S.; Searson, P. C.; Chien, C. L. *Science* **1993**, *261*, 1316.
11. Sellmyer, D. J.; Zheung, M.; Skomski, R. *J. Phys.: Condens. Matter.* **2001**, *13*, R433.
12. Piroux, L.; George, J. M.; Desperes, J. F.; Leroy, C.; Ferain, E.; Legras, R.; Ounadjela, K.; Fert, A. *Appl. Phys. Lett.* **1994**, *65*, 2484.
13. Iwasaki, T.; Motoi, T.; Den, T. *Appl. Phys. Lett.* **1999**, *75*, 2044.
14. Jeong, S.-H.; Hwang, H.-Y.; Lee, K.-H.; Jeong, Y. *Appl. Phys. Lett.* **2001**, *78*, 2052.
15. Nielsch, K.; Hertel, R.; Wehsphohn, R. B.; Bartel, J.; Kirschner, J.; Gösele, U.; Fischer, S. F.; Kronmüller, H. *IEEE Trans. Magn.* **2002**, *38*, 2571.
16. Hahn, G. C.; Zong, B. Y.; Luo, P.; Wu, Y. H. *J. Appl. Phys.* **2003**, *93*, 9202.
17. Hwang, M.; Shima, M.; Ross, C. A.; Seberino, C.; Bertram, H. N. *J. Appl. Phys.* **2002**, *92*, 1018.
18. Masuda, M.; Shomi, S.; Shiraki, M.; Egawa, H.; Murata, K. *Jpn. J. Appl. Phys.* **1987**, *26*, 1680.